ELSEVIER

Tectonophysics 333 (2001) 199–217

TECTONOPHYSICS

www.elsevier.com/locate/tecto

Present-day crustal motion along the Longitudinal Valley Fault, eastern Taiwan

Shui-Beih Yu*, Long-Chen Kuo

Institute of Earth Sciences, Academia Sinica, P.O. Box 1-55, Nankang, Taipei, Taiwan, ROC

Received 8 October 1999; revised 15 February 2000

Abstract

The NNE-striking Longitudinal Valley Fault (LVF) in eastern Taiwan is an extremely active high-angle thrust fault. It bounds the Coastal Range and the Longitudinal Valley, which is considered a collision boundary between the Philippine Sea and the Eurasian plates. Repeated GPS data in the Longitudinal Valley area from 1992 to 1999 are utilized to study the spatial variation of crustal motion along the LVF. With respect to Penghu in the Chinese continental margin, velocities for stations on the western side of the LVF (Longitudinal Valley and eastern Central Range) are 18–35 mm/yr in directions 283–311°, whereas those on the eastern side of the LVF, the Coastal Range, are 28–68 mm/yr in directions 303–324°. A major discontinuity of about 30 mm/yr on the rate of crustal motion across the Longitudinal Valley is attributed to the aseismic slip along the LVF as revealed by trilateration data previously. To the south of Fengping, the block motions of the Coastal Range are 31–40 mm/yr in 317–330° relative to the Central Range, while the near-fault motions are 13–33 mm/yr in 309–336°. Various partitions on the left-lateral strike-slip and convergent components along the LVF are found. In the southern Longitudinal Valley crustal motion is mainly accommodated on the LVF and the Luyeh Fault. In contrast, those in the central and northern Longitudinal Valley are partly taken up on the faults to the east of the LVF or result in the elastic deformation of the Coastal Range. The crustal motion in the northern Longitudinal Valley area is likely to be distributed in the several NE-striking thrusts in a horsetail pattern and obliquely cut the northern Coastal Range, with a small portion of fault-slips along the LVF. Data from dense-deployed GPS networks across the LVF can be employed to give better estimates of near-fault motions and delineate the surface traces of the LVF. Repeated GPS and leveling data from two stations on both ends of the Yuli Bridge that are 575 m apart clearly indicate that the surface trace of the LVF passes beneath the bridge with oblique horizontal motion of 23 mm/yr in 306° and uplift rate of 24 mm/yr.

Keywords: Crustal motion; Taiwan; aseismic slip; Longitudinal Valley Fault

1. Introduction

The island of Taiwan is situated at the junction between the southeast-facing Ryukyu arc-trench system and the west-facing Luzon arc-Manila Trench system (Fig. 1). The 150 km long, NNE-trending Longitudinal Valley in eastern Taiwan is widely considered an active collision boundary between the Philippine Sea and the Eurasian plates (e.g. Biq, 1972; Chai, 1972; Wu, 1978; Barrier and Angelier, 1986; Ho, 1986). It separates two quite different geologic provinces: the Central Range to the west and the Coastal Range to the east (Fig. 2). The Central Range is composed of the pre-Tertiary metamorphic

* Corresponding author. Tel.: +886-2-2783-9910 ext. 416; fax: +886-2-2783-9871.

E-mail address: eayusb@ccvax.sinica.edu.tw (S.-B. Yu).

0040-1951/01/$ - see front matter
PII: S0040-1951(00)00275-4

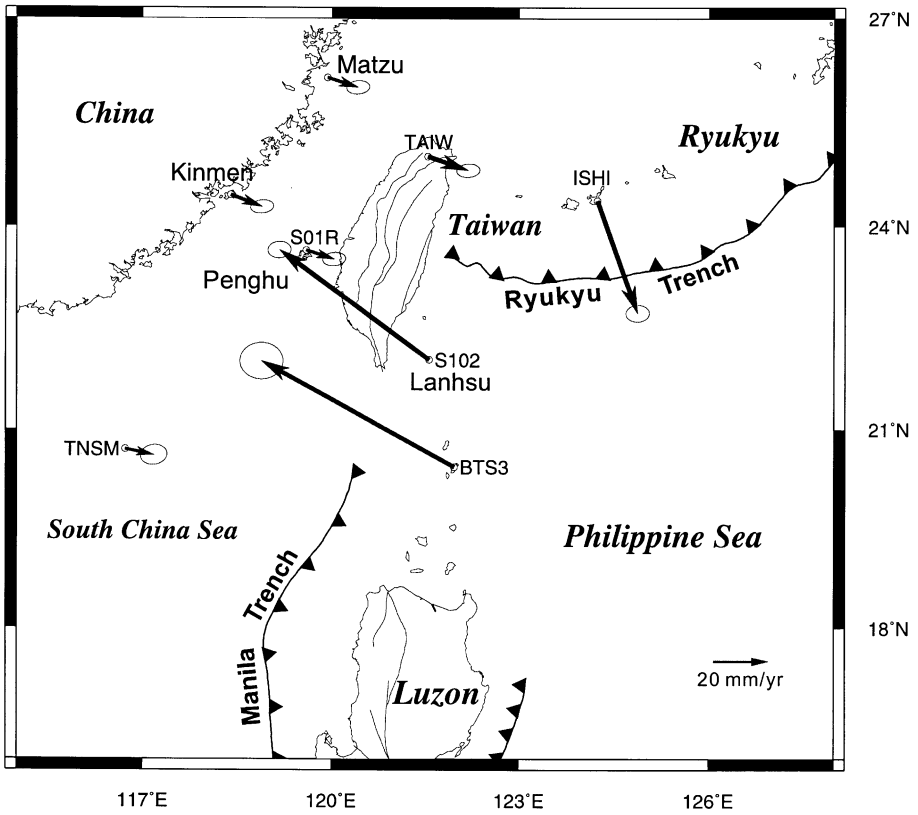

Fig. 1. Geodynamic framework around Taiwan: velocity vectors showing present-day crustal motion with respect to stable Eurasia from Yu et al. (1999). Thick lines indicate subduction with triangles on the overriding side.

basement and weakly metamorphosed Cenozoic argillite-slate series (Ho, 1986). The Coastal Range consists of Neogene andesitic volcanic units and associated flyschoid and turbidite sediments. The straight and narrow Longitudinal Valley is bounded on the east by the well-known Longitudinal Valley Fault (LVF) with the Coastal Range. The LVF is an extremely active high-angle oblique thrust fault with a minor left-lateral strike-slip component (Barrier et al., 1982; Yu and Liu, 1989).

To observe the crustal deformation across the collision boundary, five medium-aperture trilateration networks traversing the Longitudinal Valley at Hualien, Juisui, Yuli, Chihshang and Taitung have been surveyed annually since 1983. Short leveling routes in the vicinity of each trilateration network also have been surveyed annually since 1984. Analyzing repeated trilateration and leveling data, Yu and Liu (1989) found that the 50 km long central segment of the LVF, extending from Juisui south to Chihshang, is creeping significantly with both vertical and horizontal motion. Matsu'ura et al. (1986) modeled the aseismic deformation near the fault as the sum of a steady rigid block motion and the effect of an upper locked crust due to frictional resistance. Using this model, Yu et al. (1990) inverted the repeated geodetic data from the Longitudinal Valley area to determine the block motion and dislocation model parameters. The results indicate that the LVF is very weakly locked. The blocks on both sides of the fault are essentially sliding freely. The net horizontal motion across the Longitudinal Valley changes from 34 mm/yr in the direction 314° at Taitung to 25 mm/yr in the N–S direction at Hualien.

In 1989, a large-scale "Taiwan GPS Network" was established by the Institute of Earth Sciences,

Academia Sinica (IESAS). This network is now composed of more than 150 epoch-surveyed stations and nine continuously recording stations. It covers the entire island of Taiwan and several offshore islets and has been surveyed annually since 1990. Using GPS data collected prior to 1994, Yu and Chen (1994) reported that the deformation zone caused by the active collision process is more than 200 km in width. It includes a part of the Coastal Plain, Western Foothills, Central Range, Coastal Range and southeastern offshore area. The present-day velocity field of the Taiwan area was first estimated from the 1990–1995 GPS data by Yu et al. (1997). In the central and southern Coastal Range as well as two volcanic islets, Lutao and Lanhsu, the velocity vectors trend in the directions of 306–322° with rates of 56–82 mm/yr relative to Paisha, Penghu, situated on the Chinese continental margin. In contrast, a dramatic decrease in the rate of movement was detected to the north of Fengping in the northern Coastal Range. This may be attributed to the crustal motion along the NE-trending thrusts obliquely cutting the northern Coastal Range. A velocity discontinuity of about 30 mm/yr in the rates along with significant change in the directions is observed across the Longitudinal Valley.

To depict a more detailed picture for the slip distributions of the LVF and understand how the fault-slips are transferred from the LVF to the thrusts cutting the northern Coastal Range, three dense-deployed GPS networks were established at Fengping–Juisui, Yuli, and Luyeh in 1995 (Fig. 2). This study analyzes the 1992–1999 repeated GPS data from the Longitudinal Valley area and examines the variations of fault-slip along the strike of the LVF. The results from the three dense-deployed networks are also discussed.

2. Data acquisition and processing

GPS data from five continuously recording permanent stations and 45 epoch-surveyed stations on both sides of the Longitudinal Valley were used to study the spatial variation of crustal motion along the strike of the LVF (Fig. 2). Three permanent stations at Changping (S058), Mingyeh (S105) and Fushan (S104), installed by the IESAS, have been in operation since 1992. Other two permanent stations at Fenglin (FLNM) and Taimali (TMLM) operating by the Ministry of Interior (MOI) started observations in 1994 and 1995, respectively. Most of the 45 epoch-surveyed stations have been surveyed annually since 1990. Considering the availability of precise ephemerides, only data acquired since 1992 were used in this study. Three dense-deployed networks at Fengping–Juisui, Yuli, and Luyeh were set up and initially surveyed in 1996, 1995, and 1997, respectively.

In each survey, 6–12 stations were observed simultaneously with dual-frequency geodetic GPS receivers (Trimble 4000 SST Geodetic II P and 4000 SSE/SSI Geodetic Surveyor). A station is usually occupied by more than two sessions, each session consisting of 6–14 h of observation with all available healthy GPS satellites rising higher than 15° above the horizon being tracked. The sampling interval for data logging is 15 s. The downloaded raw data are transferred to Receiver INdependent EXchange (RINEX) format for use in post-processing.

The epoch measurements and continuous GPS data are incorporated and processed with the Bernese GPS software V.4.0 (Rothacher and Mervart, 1996) session by session to obtain the precise station coordinates and baseline vectors. The precise ephemerides provided by Scripps Institution of Oceanography (SIO) of the University of California at San Diego (USA) were used in the processing of the 1992 and 1993 data. Since the beginning of 1994, the final precise ephemerides distributed by the International GPS service for Geodynamics (IGS) have been employed for data processing. The solutions estimated from the fixed SIO and IGS ephemerides do not, in fact, reveal any significant differences (Yu et al., 1997). The quality of IGS final orbit is now better than 0.05 m (Rothacher and Mervart, 1996). Thus, the errors in baseline components due to orbit errors are negligible for baseline length less than 1000 km.

The ionosphere-free linear combination of carrier phase observations at the L_1 and L_2 frequencies, L_3, are utilized to remove the first-order ionospheric effects. An elevation cut-off angle of 15° is imposed to reduce any multipath effects and noise. The tropospheric refraction corrections are computed based on the Saastamoinen (1973) atmospheric zenith delay model with standard atmosphere. The residual zenith delay, which is the difference between the actual

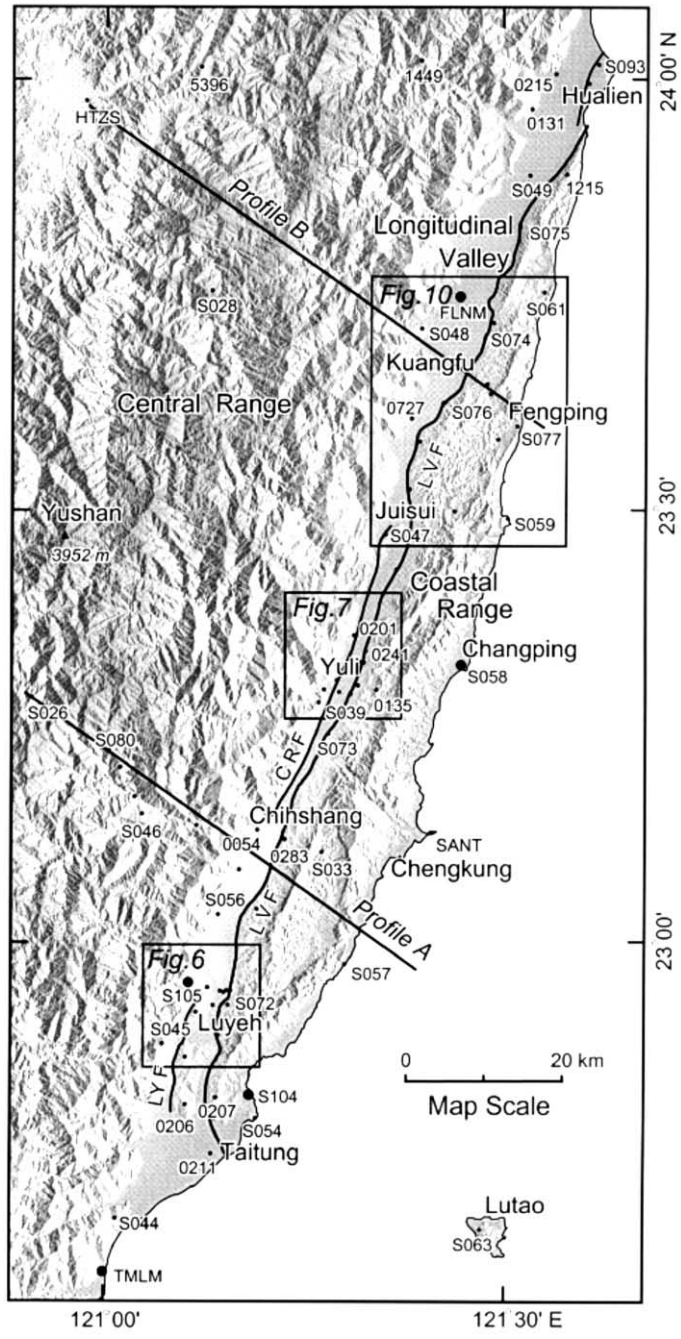

Fig. 2. GPS stations in the Longitudinal Valley area. Small dots denote epoch-surveyed stations, while large dots are continuously recording permanent stations. LVF, CRF, and LYF represent the Longitudinal Valley Fault, Central Range Fault and the Luyeh Fault respectively. Index maps for three dense-deployed GPS networks at Luyeh, Yuli and Juisui–Fengping and two profiles A and B are also shown. The topography is from a digital terrain model.

Table 1
Station velocities with respect to Paisha, Penghu in the Longitudinal Valley area (V is the station velocity; Azi is the azimuth of V; a, b are the semi-major and semi-minor axes for error ellipse of V; azi is the azimuth of a; and N is the number of campaigns)

Station	Lat. (°)	Lon. (°)	V (mm/yr)	Azi (°)	a (mm/yr)	b (mm/yr)	Azi (°)	N	Data period (yr)
To the western side of the LVF									
0216	24.023	121.631	15.8	314	0.6	0.5	76	11	92.5–99.4
1449	24.020	121.404	17.5	319	1.9	1.6	66	5	92.5–97.4
S093	24.015	121.627	16.4	314	0.8	0.7	72	7	93.4–99.4
5936	24.013	121.127	23.7	297	0.5	0.4	78	10	92.5–99.4
0215	24.005	121.573	18.1	311	1.1	0.9	68	3	95.5–99.4
MELN	23.993	121.614	27.7	312	2.1	1.7	123	3	97.1–99.4
HTZS	23.974	120.982	18.9	294	0.6	0.5	76	9	92.5–98.5
0131	23.964	121.543	20.6	309	0.5	0.4	80	10	92.5–99.4
S049	23.887	121.541	24.3	306	0.5	0.4	76	12	92.5–99.4
S028	23.752	121.143	27.2	298	1.4	1.1	100	7	94.2–98.5
FLNM	23.746	121.453	26.5	308	0.3	0.2	88	25	94.1–99.4
S048	23.710	121.405	25.8	299	0.4	0.4	78	14	92.5–99.4
0727	23.606	121.392	31.9	300	0.5	0.4	80	10	92.5–99.4
S047	23.471	121.360	34.8	308	0.4	0.3	84	14	92.5–99.4
0201	23.354	121.320	34.7	304	1.1	1.1	29	7	94.2–99.4
0713	23.323	121.327	37.9	310	1.7	1.5	22	3	96.5–99.4
13R3	23.315	121.325	43.6	306	1.8	1.7	14	5	95.2–99.4
13R4	23.302	121.299	35.0	302	1.6	1.6	17	4	95.2–99.4
1178	23.291	121.282	32.6	302	1.9	1.8	23	4	95.2–99.4
1176	23.288	121.302	33.4	305	1.7	1.6	174	3	95.2–98.3
1172	23.286	121.316	55.2	312	1.9	1.7	155	4	95.2–99.4
S026	23.282	120.916	32.5	281	0.7	0.6	72	10	92.3–98.5
S039	23.276	121.276	33.2	304	0.5	0.4	81	10	92.5–99.4
S080	23.220	121.013	32.3	288	1.0	0.9	81	9	93.4–98.3
S079	23.201	121.027	29.9	284	1.7	1.5	71	5	93.4–98.3
S078	23.167	121.045	32.4	290	1.4	0.7	90	5	93.4–99.4
S046	23.147	121.055	32.5	294	0.8	0.5	91	8	93.4–99.4
S055	23.134	121.123	32.9	294	1.1	0.7	91	7	93.4–99.4
0054	23.129	121.199	34.1	300	0.8	0.5	89	9	92.5–99.4
8046	23.083	121.176	35.7	297	1.0	0.5	90	8	92.5–99.4
S040	23.031	121.150	35.4	293	0.6	0.4	91	8	93.4–99.4
S105	22.952	121.113	33.7	293	0.3	0.3	87	22	93.4–99.4
8049	22.946	121.137	40.8	313	3.7	3.5	80	3	97.1–99.4
0308	22.942	121.161	49.1	295	2.6	2.4	123	3	97.1–99.4
S127	22.942	121.153	40.5	302	2.5	2.4	120	3	97.1–99.4
S128	22.940	121.157	40.9	306	2.4	2.3	118	3	97.1–99.4
8050	22.925	121.144	45.3	306	2.4	2.3	122	3	97.1–99.4
E908	22.917	121.123	45.1	302	2.1	2.0	113	3	97.1–99.4
S045	22.880	121.080	32.4	291	0.5	0.5	88	9	92.5–99.4
0206	22.810	121.109	47.0	280	0.6	0.6	85	7	93.4–99.4
0211	22.753	121.142	42.5	288	0.6	0.5	91	9	93.4–99.4
S044	22.678	121.022	33.2	283	0.5	0.4	90	12	92.5–99.4
TMLM	22.616	121.007	32.5	285	0.3	0.3	97	21	95.2–99.4
To the eastern side of the LVF									
1215	23.888	121.587	29.8	317	0.6	0.5	73	9	92.5–99.4
S075	23.828	121.528	28.2	313	0.7	0.6	71	6	93.4–99.4
S061	23.751	121.559	35.8	324	0.5	0.4	76	8	92.5–99.4
S074	23.716	121.495	36.1	321	0.5	0.5	76	9	92.5–99.4
8152	23.645	121.487	49.4	315	1.4	1.2	84	5	96.1–99.4

Table 1 (*continued*)

Station	Lat. (°)	Lon. (°)	*V* (mm/yr)	Azi (°)	*a* (mm/yr)	*b* (mm/yr)	Azi (°)	*N*	Data period (yr)
S099	23.634	121.491	48.5	314	1.2	1.1	73	4	96.5–99.4
S098	23.624	121.434	45.8	306	1.4	1.4	51	4	96.5–99.4
S076	23.623	121.432	44.6	298	1.2	1.0	79	5	92.5–96.5
S077	23.596	121.525	63.3	318	0.5	0.5	72	8	92.5–99.4
S100	23.581	121.501	60.2	316	1.9	1.7	102	3	97.1–99.4
S122	23.578	121.403	38.9	302	1.7	1.5	94	4	96.5–99.4
S123	23.523	121.390	41.2	304	2.1	1.9	108	3	97.1–99.4
S121	23.497	121.446	54.2	310	2.0	1.8	112	3	97.1–99.4
S059	23.488	121.513	67.0	316	0.6	0.5	77	8	92.5–99.4
0241	23.336	121.335	53.3	312	1.2	1.1	24	6	94.2–99.4
0307	23.322	121.332	60.7	308	1.9	1.7	31	3	96.5–99.4
S058	23.319	121.454	64.9	316	0.3	0.2	90	23	93.4–99.4
0242	23.296	121.325	55.9	318	1.8	1.7	12	5	95.2–99.4
0135	23.291	121.349	56.8	317	0.6	0.5	82	8	93.4–99.4
S073	23.240	121.288	57.1	308	0.6	0.4	86	9	92.5–99.4
SANT	23.125	121.416	67.8	311	0.5	0.4	92	8	93.4–99.4
0283	23.118	121.234	65.4	312	1.1	0.9	73	7	92.5–98.3
S033	23.103	121.280	64.5	312	0.6	0.5	85	7	93.4–99.4
S056	23.037	121.199	64.0	307	0.7	0.5	87	7	93.4–99.4
S057	22.973	121.309	67.0	311	0.5	0.5	91	7	93.4–99.4
S129	22.942	121.166	62.4	309	2.3	2.2	127	3	97.1–99.4
S072	22.926	121.163	64.7	305	0.5	0.5	82	7	93.4–99.4
S126	22.890	121.150	60.2	302	2.7	2.6	141	3	97.1–99.4
S104	22.821	121.189	63.2	309	0.3	0.2	93	25	93.4–99.4
0207	22.818	121.148	60.0	304	1.2	1.1	66	6	93.4–98.3
S054	22.794	121.197	64.4	307	0.6	0.5	93	7	93.4–99.4
S063	22.665	121.479	81.0	305	0.5	0.5	94	8	93.4–99.4

zenith delay and that calculated from a standard atmosphere model, is further estimated every 2 h per station (Brunner and Welsch, 1993). The coordinates of the IGS station in Taipei (TAIW, see Fig. 1) are constrained to their International Terrestrial Reference Frame 1996 (ITRF96) values.

The program ADDNEQ in the Bernese software was developed to compute multi-session solutions from the statistically correct combination of a set of single-session solutions (Rothacher and Mervart, 1996). It can also be applied to estimate the station velocity if the data set covers a long time span. The normal equations (NEQs) of single-session solutions for a campaign are first combined to create a campaign solution. An annual survey campaign in the Longitudinal Valley area usually spans 10–15 days. The multi-year campaign solutions are then combined to estimate the station velocities.

3. Spatial variation of crustal motion

The ITRF96 coordinates and velocities of three permanent stations in the Chinese continental margin (Matzu, Kinmen, and Penghu, see Fig. 1) were obtained using constraints on the coordinates and velocities of the 12 IGS fiducial stations by Yu et al. (1999). Then the ITRF96 velocities of GPS stations in the Longitudinal Valley area are estimated by constraining the coordinates and velocities of those three stations to that reported by Yu et al. (1999). The station velocities relative to Paisha, Penghu (S01R) are finally computed by subtracting S01R's ITRF96 velocity from those for the other stations. Table 1 gives the velocities relative to Paisha, Penghu and pertinent data for all GPS stations in this study. The error ellipses are obtained from properly scaled formal errors of the GPS observable inversions. They are consistent with that from long-term repeatability.

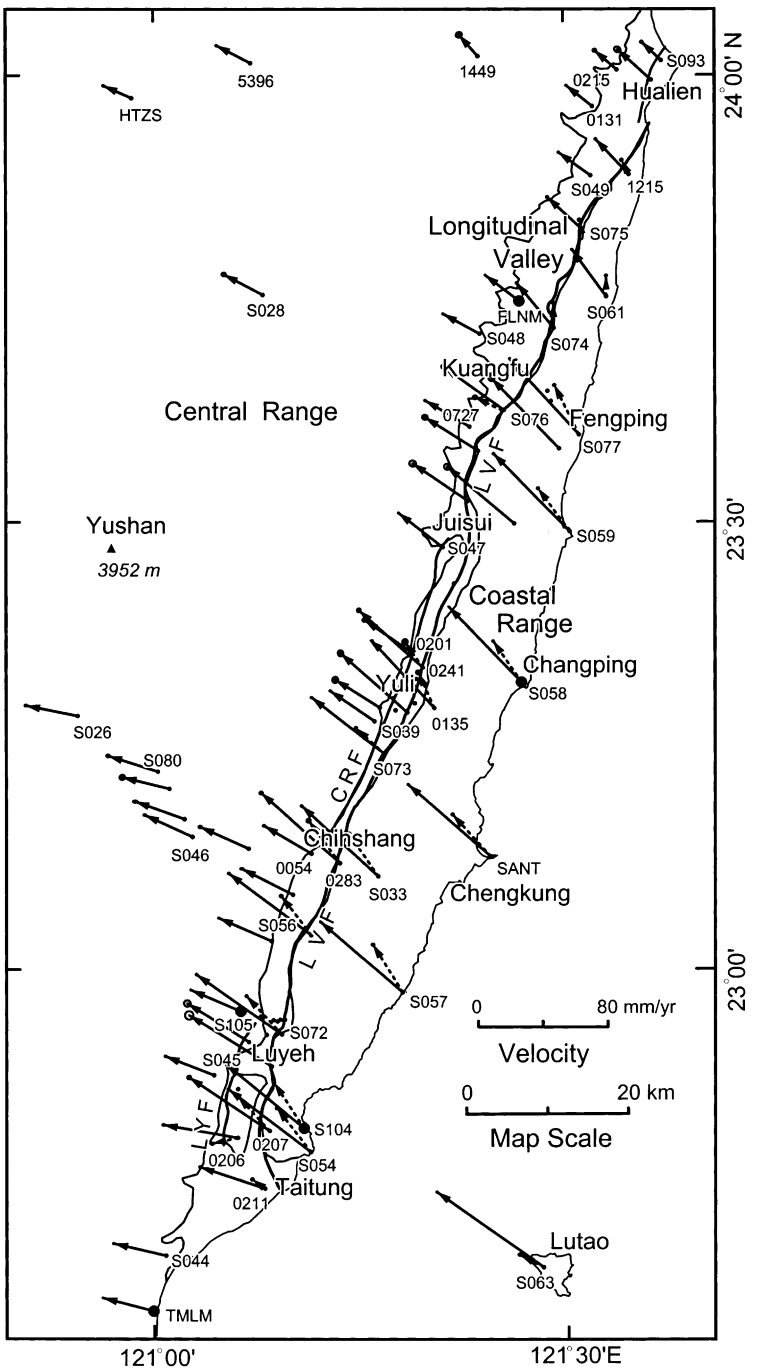

Fig. 3. Station velocities relative to Paisha, Penghu in the Longitudinal Valley area. The 95% confidence is shown at the tip of each velocity vector. The black dashed arrows in the Coastal Range are velocities with respect to the eastern margin of the Central Range.

Table 2
Fault motion along the Longitudinal Valley Fault (LVF) ($V_{AB} = V_A - V_B$; Azi is the azimuth of V_{AB}; V_p and V_n are components of V_{AB} parallel and normal to the general strike of the LVF (20°), respectively; *a* and *b* are the semi-major and semi-minor axes of the error ellipse for V_{AB}, respectively; and azi is the azimuth of *a*)

Station A	V_{AN} (mm/yr)	V_{AE} (mm/yr)	Sta B	V_{BN} (mm/yr)	V_{BE} (mm/yr)	V_{AB} (mm/yr)	Azi (°)	*a* (mm/yr)	*b* (mm/yr)	azi (°)	V_p (mm/yr)	V_n (mm/yr)
Northern segment of the LVF												
1215	21.6	−20.4	0131	12.9	−16.0	9.7	333	0.8	0.7	73	6.7	7.1
S075	19.3	−20.6	S049	14.2	−19.7	5.2	350	0.8	0.7	71	4.5	2.6
S061	29.0	−21.0	FLNM	16.1	−21.0	12.9	0	0.6	0.5	76	12.1	4.4
S074	27.9	−22.9	S048	12.4	−22.6	15.5	359	0.7	0.6	76	14.5	5.6
Central segment of the LVF												
S098	26.7	−37.2	S048	12.4	−22.6	20.4	314	1.4	1.4	91	8.4	18.6
S122	20.8	−32.9	S048	12.4	−22.6	13.3	309	1.7	1.5	66	4.4	12.5
S123	22.9	−34.2	S048	12.4	−22.6	15.6	312	2.1	1.9	66	5.9	14.5
0241	35.5	−39.7	S039	18.6	−27.5	20.8	324	1.3	1.2	66	11.7	17.2
0307	37.6	−47.6	S039	18.6	−27.5	27.7	313	2.0	1.7	66	11.0	25.4
0242	41.4	−37.5	S039	18.6	−27.5	24.9	336	1.9	1.8	66	18.0	17.2
1172	36.7	−41.3	S039	18.6	−27.5	22.8	323	1.9	1.7	66	12.3	19.1
S073	34.7	−45.3	S039	18.6	−27.5	24.0	312	0.7	0.6	86	9.1	22.2
S098	26.7	−37.2	0727	16.2	−27.5	14.3	317	1.5	1.4	91	6.5	12.7
S122	20.8	−32.9	0727	16.2	−27.5	7.1	310	1.8	1.5	91	2.5	6.6
S123	22.9	−34.2	0727	16.2	−27.5	9.5	315	2.2	1.9	91	4.0	8.6
0241	35.5	−39.7	0713	24.3	−29.1	15.4	317	2.1	1.9	91	6.9	13.8
0307	37.6	−47.6	0713	24.3	−29.1	22.8	306	2.5	2.3	91	6.2	21.9
0242	41.4	−37.5	0713	24.3	−29.1	19.1	334	2.5	2.3	91	13.2	13.7
1172	36.7	−41.3	0713	24.3	−29.1	17.4	315	2.5	2.3	91	7.5	15.7
Southern segment of the LVF												
0283	43.4	−49.0	0054	17.1	−29.5	32.7	323	1.3	1.1	73	18.1	27.3
S056	38.4	−51.2	S040	14.0	−32.5	30.7	323	0.9	0.7	87	16.6	25.9
S129	39.5	−48.3	S105	13.3	−31.0	31.4	327	2.3	2.2	66	18.7	25.2
S072	37.2	−52.9	S105	13.3	−31.0	32.4	318	0.6	0.6	82	15.0	28.7
S126	31.5	−51.3	S105	13.3	−31.0	27.3	312	2.8	2.6	66	10.2	25.3
0207	33.2	−50.0	S045	11.7	−30.2	29.2	317	1.3	1.2	66	13.5	25.9
S129	39.5	−48.3	S128	23.7	−33.3	21.8	316	3.3	3.2	91	9.7	19.5
S072	37.2	−52.9	S128	23.7	−33.3	23.8	305	2.5	2.3	91	6.0	23.0
S126	31.5	−51.3	S128	23.7	−33.3	19.6	293	3.6	3.5	91	1.2	19.6
Eastern coast												
S077	46.8	−42.6	S048	12.4	−22.6	39.8	330	0.7	0.6	72	25.5	30.5
S059	47.8	−47.0	0727	16.2	−27.5	37.1	328	0.8	0.7	77	23.1	29.1
S058	46.8	−45.0	S047	21.3	−27.5	30.9	326	0.5	0.4	90	18.0	25.1
SANT	44.4	−51.2	S039	18.6	−27.5	35.0	317	0.7	0.6	92	16.2	31.1
S057	43.5	−51.0	S040	14.0	−32.5	34.8	328	0.8	0.6	91	21.4	27.5
S104	40.0	−48.9	S105	13.3	−31.0	32.1	326	0.4	0.4	93	19.0	25.9
S054	39.0	−51.3	S045	11.7	−30.2	34.5	322	0.8	0.7	93	18.5	29.1
Northern Coastal Range												
S061	29.0	−21.0	S075	19.3	−20.6	9.7	358	0.8	0.7	76		
S077	46.8	−42.6	S074	27.9	−22.9	27.3	314	0.8	0.7	72		
S077	46.8	−42.6	S061	29.0	−21.0	28.0	310	0.7	0.6	72		
Pinanashan conglomerate and Lutao												
0207	33.2	−50.0	0206	8.1	−46.3	25.4	352	1.3	1.2	66		
S054	39.0	−51.3	0211	13.3	−40.4	27.9	337	0.8	0.7	93		
0206	8.1	−46.3	S045	11.7	−30.2	16.5	257	0.8	0.7	85		
0211	13.3	−40.4	S044	7.6	−32.4	9.8	305	0.8	0.7	91		
S063	46.7	−66.2	S054	39.0	−51.3	16.8	297	0.8	0.7	94		

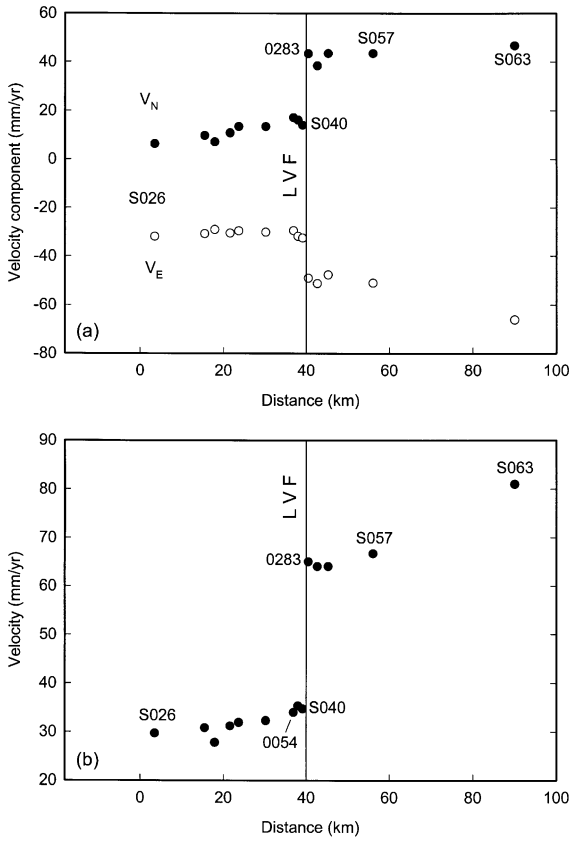

Fig. 4. (a) Variations of the north (solid circles) and east (open circle) velocity components relative to Paisha, Penghu (S01R) for Profile A, from Tienchih (S026) to Lutao (S063). The abscissa is the projected distance of each station on a line parallel to the direction of plate motion (305°). The location of the LVF is shown as a straight line. (b) Station velocities projected in the direction of plate motion for Profile A.

The velocity vectors for stations with longer observation periods (mostly from 1992 to 1999) are shown in Fig. 3. The 95% confidence ellipse is plotted at the tip of each velocity vector. To the south of Kuangfu–Fengping, the stations located in the eastern margin of the Central Range have velocities of 31.9–35.4 mm/yr, 283–304°. In contrast, stations in the Coastal Range indicate velocities of 53.3–67.8 mm/yr, 303–318°. There are dramatic decreases in the rates of crustal motion and significant westerly deviations in the motion directions across the LVF. On the other hand, remarkable decreases in station velocities are also observed to the north of Kuangfu–Fengping. The rates are only 18.1–26.5 and 28.2–36.1 mm/yr on the western and eastern sides of the LVF, respectively.

To give better estimate of crustal motion along the LVF, the velocities of stations on the western side of the LVF (V_B) are subtracted from the velocities of the nearby corresponding stations in the Coastal Range (V_A). The resultant vectors (V_{AB}), which represent the relative motion across the LVF, are given in Table 2 and also shown in Fig. 3 as dashed arrows. The crustal motions in the northern segment of the LVF are only 5.2–15.5 mm/yr in the directions 333–0°. In the central segment of the LVF, from Kuangfu to the south of Yuli, the relative motions are 13.3–24.9 mm/yr, in 309–336°. The relative fault motions across the southern segment of the LVF, from Chihshang to Taitung, increase significantly with rates of 29.2–32.7 mm/yr in the directions of 312–323°.

Along the eastern coast from Fengping to Taitung, the station velocities relative to the western side of the LVF are 30.9–39.8 mm/yr in 317–330° (Table 2), which may be taken as the velocities of the Coastal Range block with respect to the eastern margin of the Central Range. The fault motions on the southern segment of the LVF are essentially the same as the block motions of the Coastal Range, suggesting that the crustal motion is mostly taken up on the LVF. On the other hand, the velocities of fault motions along the central and northern segments of the LVF are smaller than that of the Coastal Range block. This indicates that part of crustal deformations may be accommodated on the faults other than the LVF or result in internal deformation of the Coastal Range.

The relative motions between Fengping (S077) and the northern Coastal Range (S074 and S061) are 27.3–28.0 mm/yr in 310–314°. If we take the strike of the fault obliquely cutting the Coastal Range to be in the NE direction (45°), the relative motions are essentially all convergence. As pointed out by Yu et al. (1997), this result shows that the fault-slips mainly accommodated on the central and southern segments of the LVF have transferred to the NE-striking thrusts obliquely cutting the northern Coastal Range. The idea that there may be a southward migration of the NW-vergent thrusting in the Coastal Range, as proposed by Angelier et al. (1995), seems to be supported by these GPS observations.

The relative motions between the southern Coastal

Table 3
Station velocities relative to Tienchih (S026) for a GPS profile along the South Cross-island highway (V_N and V_E are the north and east components of velocity with respect to Penghu; V is the velocity relative to Tienchih; Azi is the azimuth of V; a and b are the semi-major and semi-minor axes for error ellipse of V, respectively; and azi is the azimuth of a)

Station	V_N (mm/yr)	V_E (mm/yr)	V (mm/yr)	Azi (°)	a (mm/yr)	b (mm/yr)	azi (°)
S026	6.3	−31.9					
S080	9.7	−30.8	3.6	18	1.2	1.1	81
S079	7.1	−29.1	2.9	74	1.8	1.6	71
S078	10.8	−30.5	4.7	17	1.5	0.9	90
S046	13.4	−29.6	7.5	18	1.1	0.8	91
S055	13.4	−30.1	7.3	14	1.3	0.9	91
S105	13.3	−31.0	7.1	7	0.8	0.7	87
S040	14.0	−32.5	7.7	356	0.9	0.7	91
0054	17.1	−29.5	11.1	12	1.1	0.8	89
8046	16.1	−31.8	9.8	1	1.2	0.8	90
0283	43.4	−49.0	40.9	335	1.3	1.1	73
S056	38.4	−51.2	37.5	329	1.0	0.8	87
S033	43.5	−47.6	40.4	337	0.9	0.8	85
S057	43.5	−51.0	41.8	333	0.9	0.8	91
SANT	44.4	−51.2	42.7	333	0.8	0.7	92

Range (0207, S054) and the Pinanshan conglomerate (0206, 0211) are 25.4–27.9 mm/yr in 337–352°. Considering the local strike of the LVF has changed to be more or less in the N–S direction here, the fault motions are mostly left-lateral strike-slip. On the contrary, there are moderate convergences of 9.5–13.9 mm/yr between the Pinanshan conglomerate and the Central Range. Based on trilateration data and geological observations, Yu et al. (1992) and Lee et al. (1998) obtained similar conclusions. A significant shortening of 16.8 mm/yr in 297° is also observed between the volcanic island, Lutao, (S063) and the southern Coastal Range (S054).

A dense GPS profile from the station at Tienchih (S026) located near the highest ridge of the Central Range, traversing the Longitudinal Valley, Coastal Range to Lutao has been surveyed annually since 1993 (Profile A in Fig. 2). The variations of the north and east velocity components with respect to Paisha, Penghu (S01R) for stations along Profile A are shown in Fig. 4(a). The abscissa is the projected distance of each station on a line parallel to the motion direction of Lutao, 305°, which is very close to the direction of the Philippine Sea plate motion. There are major discontinuities of 26 and 16 mm/yr on the north and east components, respectively. The velocities projected to the direction 305° are plotted in Fig. 4(b). A slight eastward increase in the projected velocities is observed in the eastern Central Range and Coastal Range. A large velocity jump of 31 mm/yr is found across the LVF. This is mainly due to the aseismic slip (or creep) on the LVF, as noted in previous studies (e.g. Yu and Liu, 1989; Yu et al., 1990; Yu and Chen, 1994).

Based on detailed surveys of faulted concrete structures along the Chihshang Fault, which is a segment of the LVF, Angelier et al. (1997) determined average motion vectors trending 323° with an average shortening of 22 mm/yr. The GPS derived slip rate at Chihshang (31 mm/yr) is significantly larger than that determined from outcrop-scale measurements (22 mm/yr). This may be attributed to the fact that the spacing between GPS stations is usually several kilometers and the observed rate is likely to include the slips on the other faults and part of elastic deformation in the area.

The velocities of the stations in Profile A relative to the station at Tienchih (S026) are calculated as presented in Table 3 and shown in Fig. 5. The stations to the east of the LVF have velocities of 37.5–42.7 mm/yr in directions of 329–337°, while those in the eastern margin of the Central Range show much smaller velocities of 7.1–11.1 mm/yr, in 356–18°. Moderate left-shear deformations approximately

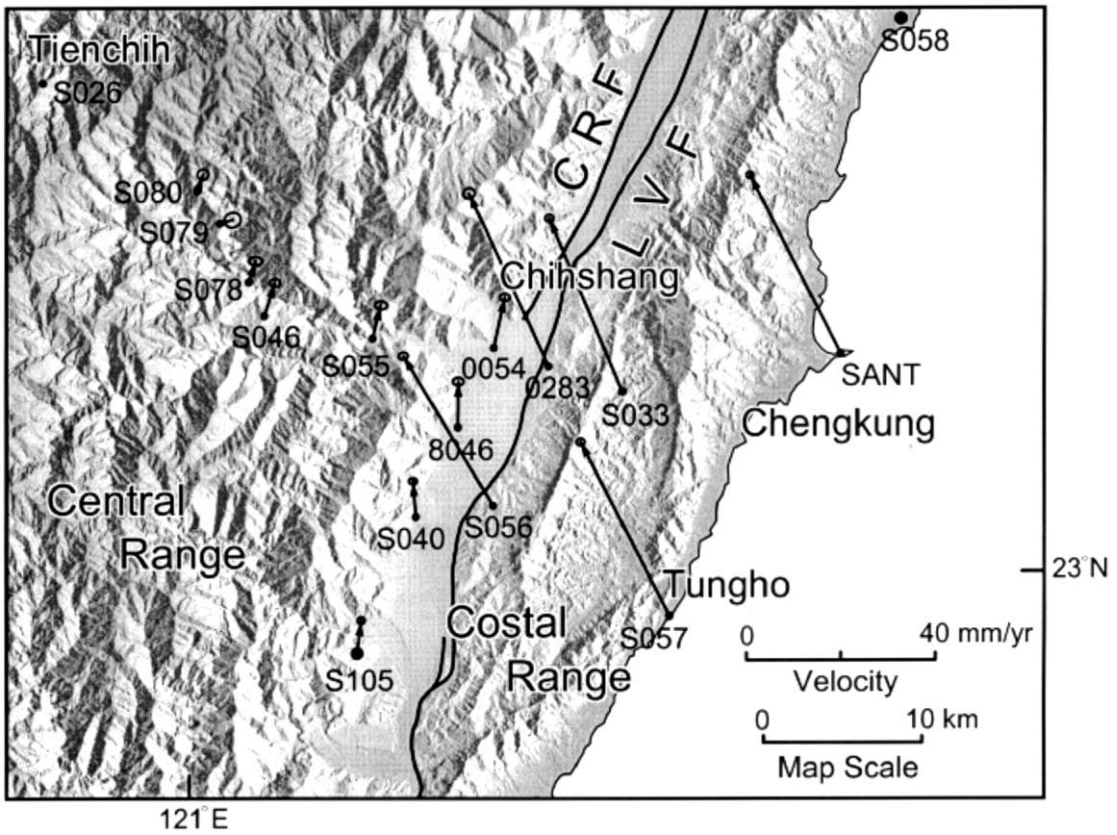

Fig. 5. Station velocities relative to Tienchih (S026) for a dense GPS profile along the Southern Cross-island highway. The 95% confidence is shown at the tip of each velocity vector. CRF denotes the Central Range Fault.

Table 4
Station velocities relative to Mingyeh (S105) for the Luyeh dense network (V_N and V_E are the north and east components of velocity with respect to Penghu; V is the velocity relative to Mingyeh; Azi is the azimuth of V; a and b are the semi-major and semi-minor axes for error ellipse of V, respectively; and azi is the azimuth of a)

Station	V_N (mm/yr)	V_E (mm/yr)	V (mm/yr)	Azi (°)	A (mm/yr)	b (mm/yr)	azi (°)
S105	13.3	−31.0					
S045	11.7	−30.2	1.8	153	0.6	0.5	88
I138	19.6	−44.8	15.2	295	2.3	2.2	108
E908	24.0	−38.2	12.9	326	2.1	2.0	113
8049	28.0	−29.7	14.8	5	3.7	3.5	80
8050	26.7	−36.6	14.5	337	2.4	2.3	122
S126	31.5	−51.3	27.3	312	1.4	1.3	141
S127	21.3	−34.4	8.7	337	2.5	2.4	120
S128	23.7	−33.3	10.7	348	2.4	2.3	118
0308	21.0	−44.4	15.5	300	2.6	2.4	123
S072	37.2	−52.9	32.4	318	0.6	0.6	82
S129	39.5	−48.3	31.4	327	2.3	2.2	127

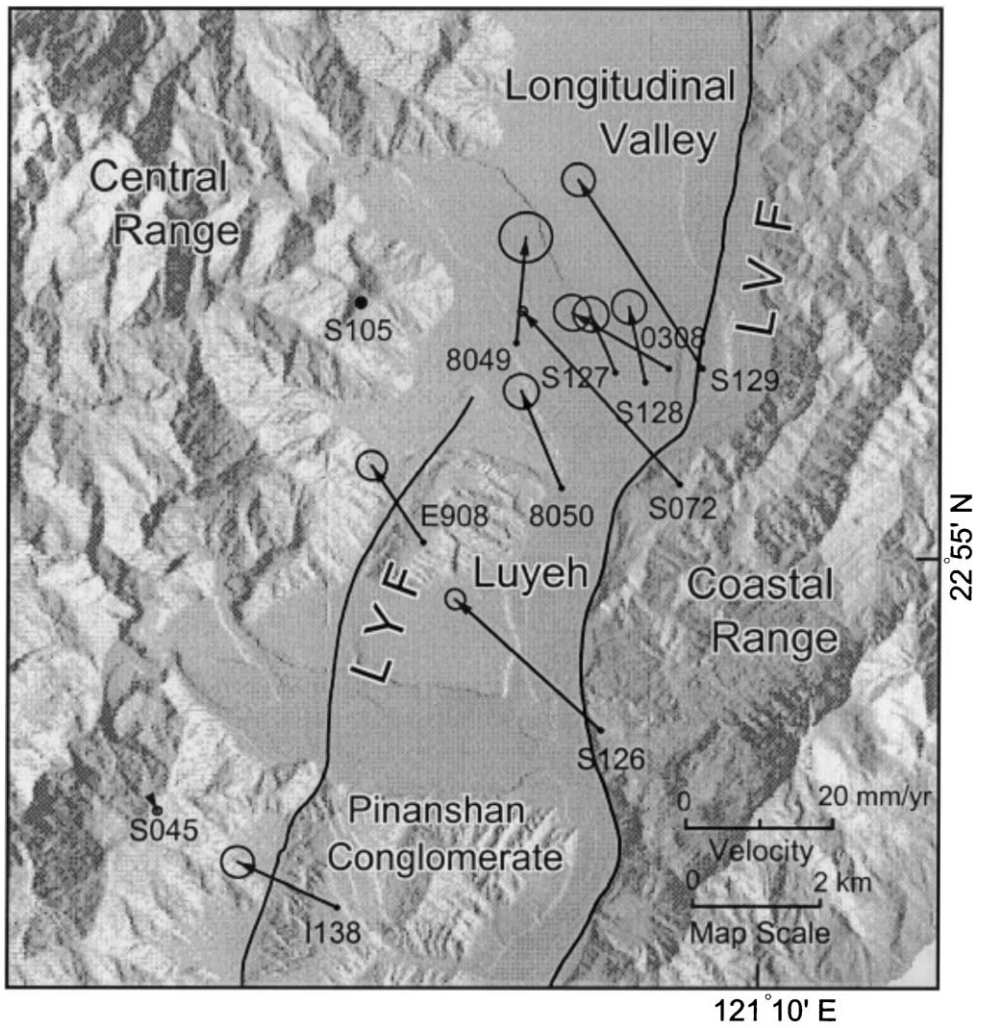

Fig. 6. Station velocities relative to Mingyeh (S105) for the Luyeh dense network. Notations are the same as in Fig. 5. LYF is the Luyeh Fault.

parallel to the strike of the LVF are observed in the eastern Central Range. This suggests that the NEE–SWW extensional deformation in the southern Central Range, as reported by Yu and Chen (1994), is not significant here.

4. Dense-deployed GPS networks

4.1. Luyeh network

Nine stations in the Luyeh area of the southern Longitudinal Valley have been dense-deployed and surveyed annually since 1997. Based on the GPS data of three surveys from 1997 to 1999, the preliminary velocity estimates of these stations relative to Paisha are given in Table 1. The differential crustal motions are computed with respect to the permanent station at Mingyeh (S105) in the eastern margin of the Central Range (see Table 4 and Fig. 6). Discontinuities in station velocities across the LVF are clearly shown. For instance, stations S128 and S129 are about 1 km apart, and the velocity of S129 relative to S128 is 21.8 mm/yr in 316°. The station (0308), located between these two stations indicates larger rate and significant deviation in the moving direction. Whether

Table 5
Station velocities relative to Changliang (S039) for the Yuli dense network (V_N and V_E are the north and east components of velocity with respect to Penghu; V is the velocity relative to Changliang; Azi is the azimuth of V; a and b are the semi-major and semi-minor axes for error ellipse of V, respectively; and azi is the azimuth of a)

Station	V_N (mm/yr)	V_E (mm/yr)	V (mm/yr)	Azi (°)	a (mm/yr)	b (mm/yr)	azi (°)
S039	18.6	−27.5					
0201	19.6	−28.7	1.6	310	1.2	1.2	29
1178	17.2	−27.7	1.4	188	2.0	1.9	23
13R4	18.7	−29.6	2.1	273	1.7	1.6	17
1176	19.3	−27.2	0.8	23	1.8	1.7	174
0713	24.3	−29.1	5.9	344	1.7	1.6	22
13R3	25.6	−35.3	10.5	312	1.9	1.8	14
1172	36.7	−41.3	22.8	323	1.9	1.7	155
0241	35.5	−39.7	20.8	324	1.3	1.2	24
0242	41.4	−37.5	24.9	336	1.9	1.8	12
0307	37.6	−47.6	27.7	313	2.0	1.7	31
0135	41.7	−38.6	25.6	334	0.8	0.7	82

this phenomenon is due to the complexity of the crustal motion near the fault zone or local instability of the geodetic marker can only be clarified through further observation. Significant convergence of 13–15 mm/yr in 295–326° is also found between the Luyeh terrace (E908) — Pinanshan conglomerate (I138) and the Central Range (S105, S045). The Luyeh Fault (LYF), at the boundary of these geologic units, may take up the major part of the observed convergence.

4.2. Yuli network

The dense GPS network at Yuli was deployed in 1995 and was surveyed 3–5 times between 1995 and 1999. The velocities relative to station S039 of the Central Range are calculated and given in Table 5 and also shown in Fig. 7. The stations situated to the east of the LVF (0241, 0307, 0242, 1172, and 0135) have velocities of 20.8–27.7 mm/yr, in directions of 313–336°. Two stations, 0713 and 0307, 575 m apart, are located right on both ends of the Yuli Bridge beneath which the surface trace of the LVF passes (Yu and Liu, 1989). The velocity of the station at the eastern end of the bridge (0307) relative to the station at the western end (0713) is 22.8 mm/yr in 306°. This velocity can be taken as the near-fault horizontal motion along the main trace of the LVF. It indicates a left-lateral strike-slip motion of 6.2 mm/yr and a convergence of 21.9 mm/yr. The horizontal creeping rate of the LVF at Yuli is essentially equal to that at Chihshang as reported by Angelier et al. (1997).

The motion of the Coastal Range block relative to the Central Range is 31–35 mm/yr. Thus, there is still about one-third of the fault-slips which is either accommodated on other faults or leads to elastic deformation in the Yuli area. No significant horizontal deformation is observed across the Central Range Fault (CRF), which is mainly delineated from the lineaments of topographic features.

A short leveling route traversing the Longitudinal Valley at Yuli (see Fig. 7) was surveyed 10 times using the procedures of first-order precise leveling from 1985 to 1996. Yu and Liu (1989) presented results using data collected prior to 1988. Fig. 8 shows the elevation changes of benchmarks relative to station 0713. A slight uplift rate of 4.5 ± 0.5 mm/yr is found to the west of the LVF. The eastern side of the LVF is steadily uplifting relative to the western side. The time variation in the elevation changes between stations 745 and 0713 is quite uniform with uplift rates of 24.4 ± 0.3 mm/yr (Fig. 9). A small portion of the uplift occurs just slightly to the east of the LVF, probably within 2 km. Thus, at the Yuli Bridge the whole reverse slip rate of the LVF is 33.4 mm/yr, which is also in agreement with the estimate of Angelier et al. (1997) at Chihshang.

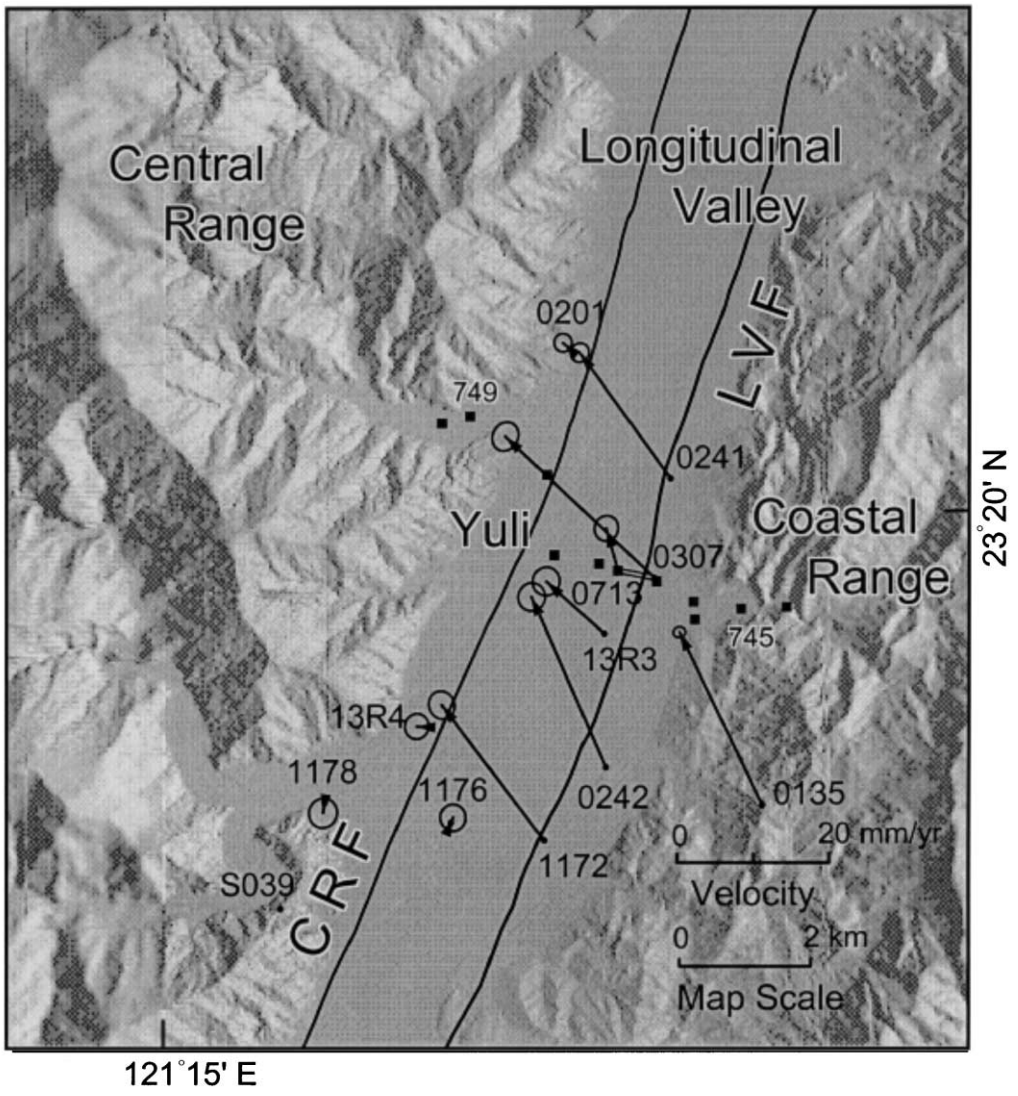

Fig. 7. Station velocities relative to Changliang (S039) for the Yuli dense network. Notations are the same as in Fig. 5.

4.3. Fengping–Juisui network

In order to study how the fault-slips are transferred from the LVF to the NE-striking thrusts cutting the northern Coastal Range, seven stations were deployed in the Fengping–Juisui area in 1996. Since then, these stations and other older ones in the area have been surveyed annually. The velocity field relative to station S048 in the Central Range is shown in Fig. 10 and the velocity components are given in Table 6. The rates of northwesterly crustal motions increase toward the east. The stations to the west of the LVF (FLNM, 0727, and S047) show velocities of 4.0–10.2 mm/yr in 308–23°. Three stations (S098, S122, and S123) immediately to the east of the LVF have velocities of 13.3–20.4 mm/yr in 309–314°. In the central part of the Coastal Range (S099, 8152, and S121), velocities of 24.6–29.4 mm/yr in 320–332° are found. Further to the east near the coast, the velocities of three stations (S100, S077, and S059) are 36.4–43.0 mm/yr in 326–330°. In contrast, two stations in the northern Coastal Range show velocities

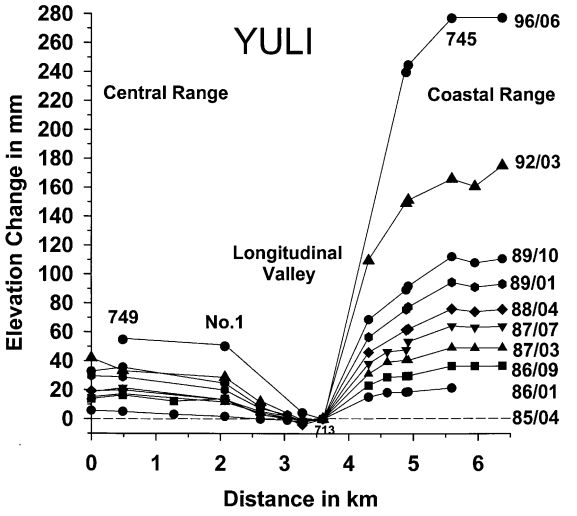

Fig. 8. Elevation changes of benchmarks relative to BM 713 in the Yuli leveling route from 1985 to 1996.

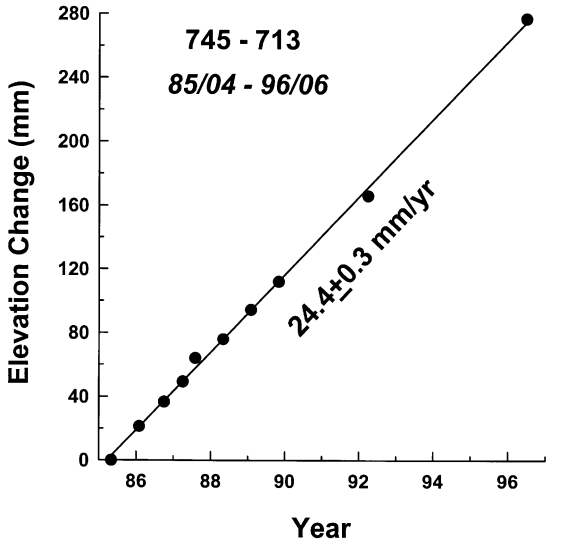

Fig. 9. Time variation plot for elevation changes between BM 745 and BM 713 from 1985 to 1996.

of 15.5–16.7 mm/yr in 359–6°. This pattern of crustal motions in the Fengping–Juisui area indicates that this segment of the LVF is no longer taken up the major part of the fault-slips. The crustal deformation is likely to be distributed in the several NE-trending thrust faults obliquely cutting the Coastal Range. These faults may in fact split from the LVF near Juisui and their surface traces indicate a horsetail pattern.

Fig. 11 shows the velocities relative to Penghu (S01R) projected in the 305° direction for the profile from Puli (HTZS) in central Taiwan to Shihtiping (S059) on the eastern coast (Profile B in Fig. 2). There is a westward decrease in velocity in the Western Foothills (S028–HTZS), implying the area has been undergoing compressive tectonic stress and resulting in E–W shortening. No significant velocity change in the eastern Central Range is detected. Then the projected velocities increase rapidly from the eastern margin of the Central Range toward the eastern coast. This suggests that there may be elastic deformation in the area or that the fault-slips are accommodated on several other faults.

5. Discussion and conclusions

The spatial variation of present-day crustal motion along the Longitudinal Valley Fault can be realized based on the repeated GPS data from 1992 to 1999. The relative velocities for the station pairs on both sides of the LVF and nearly adjacent to the fault represent the near-fault-slips, while those for station pairs far from the LVF can be taken as the velocities of the rigid Coastal Range block with respect to the eastern margin of the Central Range. The velocity components parallel (V_p) and normal (V_n) to the general strike of the LVF, i.e. 20°, are calculated and also presented in Table 2 and Fig. 12. If the estimated near-fault-slips are mainly accommodated on the LVF, the V_p and V_n indicate the strike-slip and convergent components of fault motion, respectively. The V_p and V_n for stations along the eastern coast (triangles in Fig. 12) are more or less at a constant level. On the other hand, the left-lateral slips (V_p) and convergence (V_n) of the near-fault motion (solid circles in Fig. 12) mostly have lower values than those on the eastern coast and show a northward decrease in the rates. In the southern segment of the LVF, from Taitung to Chihshang, the near-fault-slip rates on the LVF are very close to the block motion of the Coastal Range. This indicates that there is no significant deformation in the southern Coastal Range. In contrast, the near-fault-slip rates in the central and northern segments of

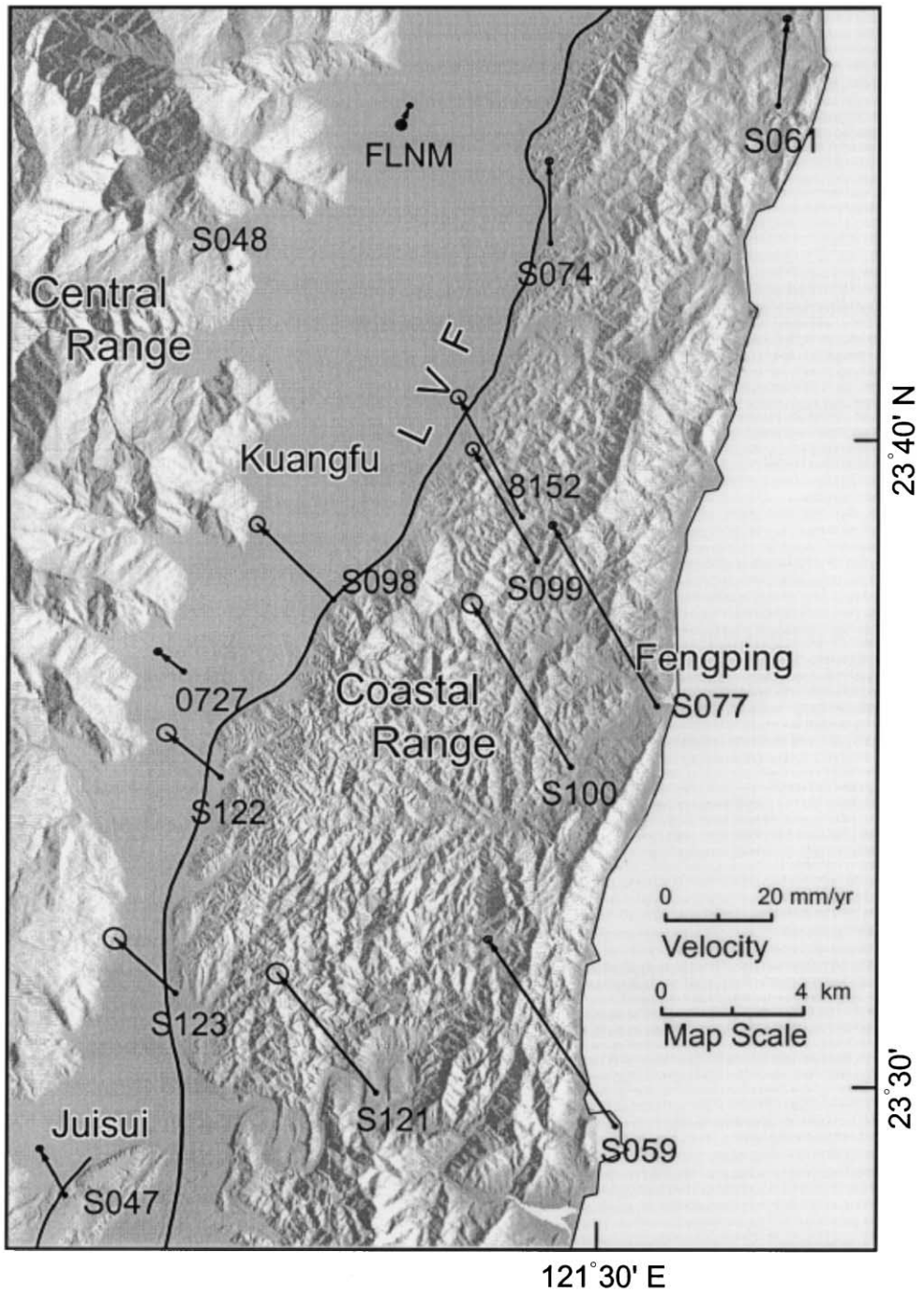

Fig. 10. Station velocities relative to Mingli (S048) for the Fengping–Juisui network. Notations are the same as in Fig. 5.

Table 6
Station velocities relative to Mingli (S048) for the Fengping–Juisui network (V_N and V_E are the north and east components of velocity with respect to Penghu; V is the velocity relative to Mingli; Azi is the azimuth of V; a and b are the semi-major and semi-minor axes for error ellipse of V, respectively; and azi is the azimuth of a)

Station	V_N (mm/yr)	V_E (mm/yr)	V (mm/yr)	Azi (°)	a (mm/yr)	b (mm/yr)	azi (°)
S048	12.4	−22.6					
FLNM	16.1	−21.0	4.0	23	0.5	0.4	88
0727	16.2	−27.5	6.2	308	0.7	0.6	80
S047	21.3	−27.5	10.2	331	0.6	0.5	84
S122	20.8	−32.9	13.3	309	1.7	1.5	94
S074	27.9	−22.9	15.5	359	0.7	0.6	76
S123	22.9	−34.2	15.6	312	2.1	1.9	108
S061	29.0	−21.0	16.7	5	0.7	0.6	76
S098	26.7	−37.2	20.4	314	1.4	1.4	51
S099	33.7	−34.9	24.6	330	1.3	1.2	73
8152	35.1	−34.8	25.8	332	1.4	1.3	84
S121	34.9	−41.5	29.4	320	2.0	1.8	112
S100	43.5	−41.6	36.4	329	1.9	1.8	102
S077	46.8	−42.6	39.8	330	0.7	0.6	72
S059	47.8	−47.0	43.0	325	0.7	0.6	77

the LVF are smaller than the block motion. The discrepancy of the slip rate is likely to be taken up on the other faults to the east of the LVF or caused by the elastic deformation in the Coastal Range. More observations at dense-deployed GPS stations and further numerical modeling studies may help clarify this uncertainty.

The near-fault motion relative to the stations immediately on the western side of the LVF for ten stations in the dense GPS networks are also estimated and given in Table 2. These data are good estimates of the fault-creep. The horizontal creep rates are 15–24 mm/yr at Luyeh and Yuli, but only 7–14 mm/yr from Juisui to Kuangfu. If the fault-creep is decomposed into the two components of left-lateral slip and convergence, the partition between them varies with the local strike of the LVF (open circles in Fig. 12).

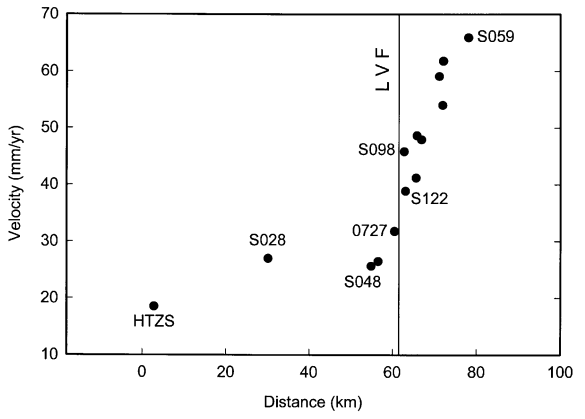

Fig. 11. Station velocities projected in the direction of plate motion (305°) for Profile B, from Puli (HTZS) to Shihtiping (S059). The location of the LVF is shown as a straight line.

As shown in Fig. 1, the summation of the east-southeast motion of the Chinese continental margin at rates of 11–12 mm/yr with respect to stable Eurasia and northwestward motion of the Luzon arc at the rate of about 70 mm/yr gives a high convergence of more than 80 mm/yr across the active Taiwan arc–continent collision zone (Yu et al., 1999). The relative motion between the Coastal Range and the eastern margin of the Central Range is approximately 35 mm/yr. In other words, about 43% of total shortening are distributed in the Longitudinal Valley and Coastal Range, and most of the deformation is attributed to the aseismic slip on the LVF.

Data from dense-deployed GPS networks across the LVF are able to delineate or provide constraints on the surface traces of the LVF. For instance, repeated GPS data from two stations on both ends of the Yuli Bridge demonstrate that the surface trace of the LVF passes beneath the bridge, and the data also provide a good

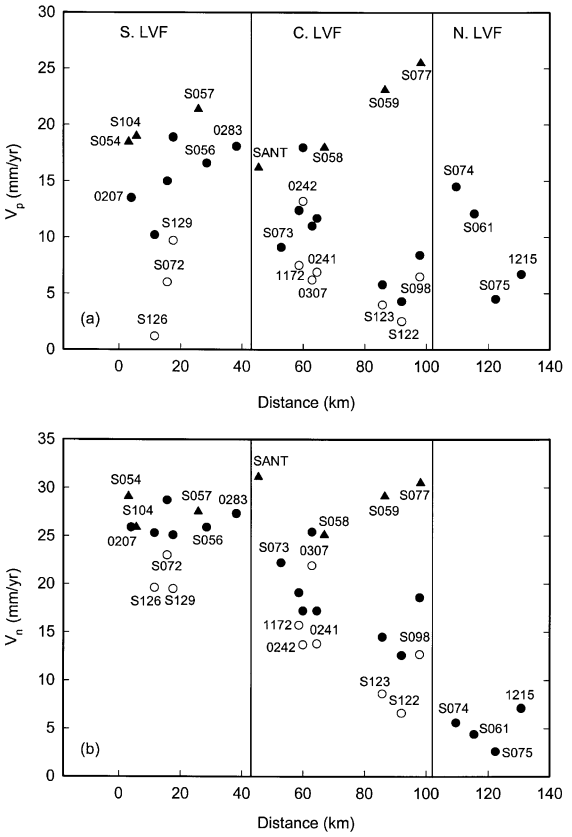

Fig. 12. Velocity components parallel (V_p) and normal (V_n) to the general strike of the LVF (20°). Triangles denote the stations along the eastern coast. Solid and open circles represent V_p and V_n, respectively, for the stations adjacent to the LVF with respect to the eastern margin of the Central Range and the nearest stations in the Longitudinal Valley.

estimate of near-fault motion. Repeated precise leveling data also show a uniform uplift rate of 24.4 mm/yr with the eastern side moving up, consistent with the results from GPS observations. GPS data along the Southern Cross-island highway indicate that there is 7–11 mm/yr of N to NNE-trending left-shear deformation in the eastern Central Range.

In the Yuli area, no significant horizontal motion is detected across the CRF located more or less along the eastern margin of the Central Range. However, there is moderate convergence of 13–15 mm/yr across the Luyeh Fault, the boundary between the Central Range and the Luyeh terrace–Pinanshan conglomerate.

In the Fengping–Juisui area, the rates of northwesterly crustal motion with respect to the central Range increase from the Longitudinal Valley toward the eastern coast. The crustal deformation is likely to be distributed in the several NE-striking thrusts with a horsetail pattern obliquely cutting the northern Coastal Range. In summary, our study shows that detailed geologic field surveys along with the deployment of additional dense GPS stations are required to identify which faults take up the active deformation.

Acknowledgements

We are grateful to many of our colleagues at IESAS and the part-time assistants for their participation in the GPS field surveys and acquisition of continuous GPS data from permanent stations. The generous provision of continuous GPS data for this study by the Ministry of Interior, R.O.C. and precise ephemerides for data processing by the Scripps Institution of Oceanography (SIO), USA and the International GPS Service for Geodynamics (IGS) community are greatly appreciated. The authors are indebted to Professors X. Le Pichon and E. Calais for their valuable comments and suggestions. Thanks are also due to Ms Y.J. Hsu and Mr H.H. Su for preparing the illustrations and tables of this manuscript. This study was financially supported by Academia Sinica and the National Science Council of the Republic of China under grant NSC 88-2116-M-001-030. This is a contribution of the Institute of Earth Sciences, Academia Sinica, IESEP2000-005.

References

Angelier, J., Lee, J.C., Chu, H.T., Lu, C.Y., Fournier, M., Hu, J.C., Lin, N.T., Deffontaines, B., Delcaillau, B., Lacombe, O., Lee, T.Q., 1995. Crustal extension in an active orogen: Taiwan (extended abstract). International Conference and Third Sino-French Symposium on Active Collision in Taiwan, 22–23 March 1995, Taipei, Taiwan, pp. 25–32.

Angelier, J., Chu, H.T., Lee, J.C., 1997. Shear concentration in a collision zone: kinematics of the Chihshang Fault as revealed by outcrop-scale quantification of active faulting, Longitudinal Valley, eastern Taiwan. Tectonophysics 274, 117–143.

Barrier, E., Angelier, J., 1986. Active collision in eastern Taiwan: the Coastal Range. Tectonophysics 125, 39–72.

Barrier, E., Angelier, J., Chu, H.T., Teng, L.S., 1982. Tectonic

analysis of compressional structure in an active collision zone: the deformation of Pinanshan Conglomerates, eastern Taiwan. Proc. Geol. Soc. China 25, 123–138.

Biq, C.C., 1972. Dual trench structure in the Taiwan–Luzon region. Proc. Geol. Soc. China 15, 65–75.

Brunner, F.K., Welsch, W.M., 1993. Effects of the troposphere on GPS measurements. GPS World 4, 42–51.

Chai, B.H., 1972. Structure and tectonic evolution of Taiwan. Am. J. Sci. 272, 389–432.

Ho, C.S., 1986. A synthesis of the geologic evolution of Taiwan. Tectonophysics 125, 1–16.

Lee, J.C., Angelier, J., Chu, H.T., Yu, S.B., Hu, J.C., 1998. Plate-boundary strain partitioning along the sinistral collision suture of the Philippine and Eurasian plates: analysis of geodetic data and geological observation. Tectonics 17, 859–871.

Matsu'ura, M., Jackson, D.D., Cheng, A., 1986. Dislocation model for aseismic crustal deformation at Hollister, California. J. Geophys. Res. 91, 12661–12674.

Rothacher, M., Mervart, L. (Eds.), 1996. Bernese GPS software V.4.0, Astronomical Institute, University of Berne, Switzerland, 418 pp.

Saastamoinen, I.I., 1973. Contribution to the theory of atmospheric refraction. Bull. Geodesique 107, 13–34.

Wu, F.T., 1978. Recent tectonics in Taiwan. J. Phys. Earth 26, S265–S299.

Yu, S.B., Chen, H.Y., 1994. Global Positioning System measurements of crustal deformation in the Taiwan arc–continent collision zone. TAO 5, 477–498.

Yu, S.B., Liu, C.C., 1989. Fault creep on the central segment of the Longitudinal Valley fault, eastern Taiwan. Proc. Geol. Soc. China 32, 209–231.

Yu, S.B., Jackson, D.D., Yu, G.K., Liu, C.C., 1990. Dislocation model for crustal deformation in the Longitudinal Valley area, eastern Taiwan. Tectonophysics 183, 97–109.

Yu, S.B., Yu, G.K., Kuo, L.C., Lee, C., 1992. Crustal deformation in the southern Longitudinal Valley area, eastern Taiwan. J. Geol. Soc. China 35, 219–230.

Yu, S.B., Chen, H.Y., Kuo, L.C., 1997. Velocity field of GPS stations in the Taiwan area. Tectonophysics 274, 41–59.

Yu, S.B., Kuo, L.C., Punongbayan, R.S., Ramos, E.G., 1999. GPS observation of crustal deformation in the Taiwan–Luzon region. Geophys. Res. Lett. 26, 923–926.